ELSEVIER

Marine and Petroleum Geology 20 (2003) 13–27

Marine and Petroleum Geology

www.elsevier.com/locate/marpetgeo

# Influence of differential compaction above basement steps on salt tectonics in the Ligurian-Provençal Basin, northwest Mediterranean

Agnès Maillard[a,*], Virginie Gaullier[b], Bruno C. Vendeville[c], Francis Odonne[a]

[a]*LMTG, UMR CNRS 5563, Université Paul Sabatier, 39, Allées Jules Guesde, 31062 Toulouse, France*
[b]*Laboratoire d'étude des Géoenvironments marins (LEGEM), Université de Perpignan, 52, avenue de Villeneuve, 66860 Perpignan, France*
[c]*Bureau of Economic Geology, The University of Texas at Austin, University Station, Box X, Austin, TX 78713, USA*

Received 12 July 2002; received in revised form 16 February 2003; accepted 12 March 2003

**Abstract**

Detailed mapping of the Ligurian-Provençal Basin (northwestern Mediterranean) indicates that salt diapirs in the deep basin are restricted to an area whose upslope boundary forms reentrants located above deep crustal transfer zones associated with the opening of the basin in Oligo–Miocene times. Because these basement faults were no longer active in Messinian and post-Messinian times, the geographic correlation between diapirs and basement faults cannot be attributed to slip along these basement faults coeval with salt tectonics. Using three physical experiments, we examine how dormant (i.e. inactive) basement steps can affect the development of the overlying salt structures during combined gravity-driven gliding and spreading. Where a basement step trends obliquely with respect to the direction of the slope and initially offsets the base salt, grabens and salt ridges form above and downdip from the basement step, in turn forming a reentrant pointing upslope. Where the basement step is buried under pre-Messinian compactable sediments, loading by Messinian and post-Messinian sediments causes differential subsidence above the step, forcing grabens and salt ridges to form above and updip of the basement step. There, too, the salt structures are confined in a triangular, reentrant-shaped area pointing upslope. The combination of these two mechanisms with passive diapir growth during Plio-Pleistocene times explains the striking geographic correlation between salt diapirs and basement structures in the Gulf of Lion.


*Keywords:* Analogue modeling; Gulf of Lion; Transfer faults; Compaction; Salt diapirs

## 1. Introduction

The opening of the Liguro-Provençal Basin, northwest Mediterranean, during Oligo–Miocene times is responsible for the southeastward drift and rotation of the Corsica-Sardinia block along transfer zones (Biju-Duval, 1984; Le Douaran, Burrus, & Avedik, 1984; Réhault, Boillot, & Mauffret, 1984; Fig. 1). The postrift sedimentary cover of the basin includes a thick, highly mobile layer of Messinian halite (Ryan & Hsu, 1973) that allowed for vigorous salt tectonics and diapirism (Gaullier & Bellaiche, 1996).

In this article, we first review data from previous work to demonstrate that there is a spatial correlation between the location and orientation of both the salt-diapir reentrants and the transfer zones in the pre-Messinian basement. We then use results from analogue modeling to explain which mechanisms may be responsible for this peculiar correlation.

## 2. Geological setting

The opening of the Ligurian-Provençal Basin was a short-lived tectonic event occurring in the general framework of the slow convergence between the African and European plates (Dewey, Helman, Turco, Hutton, & Knott, 1989; Olivet, 1996). By analogy with the marginal basins of the western Pacific Ocean, the origin of the Ligurian-Provençal Basin is commonly attributed to back-arc spreading during northwestward subduction of the African plate (Réhault et al., 1984) and the associated retreat of the subducting slab toward the Appenines and Calabria (Doglioni, Gueguen, Harabaglia, & Mongelli, 1999; Gueguen, Doglioni, & Fernandez, 1997; Malinverno & Ryan, 1986).

* Corresponding author.
*E-mail address:* maillard@cict.fr (A. Maillard).

0264-8172/03/$ - see front matter © 2003 Elsevier Science Ltd. All rights reserved.
doi:10.1016/S0264-8172(03)00022-9

Rifting in the Ligurian-Provençal Basin took place from late Oligocene to early Miocene times and was followed by seafloor spreading during Aquitanian and Burdigalian times. As it rotated counterclockwise, the Corsica-Sardinia continental block split from the European mainland, thus widening the triangular Ligurian-Provençal Basin during Miocene time (Guegen, 1996; Le Douaran et al., 1984; Mauffret, Pascal, Maillard, & Gorini, 1995; Montigny, Edel, & Thuizat, 1981; Réhault et al., 1984; Speranza et al., 2002; Vigliotti & Langenheim, 1995).

The Gulf of Lion (Fig. 1), which represents the northwest continental margin of the Ligurian-Provençal Basin,

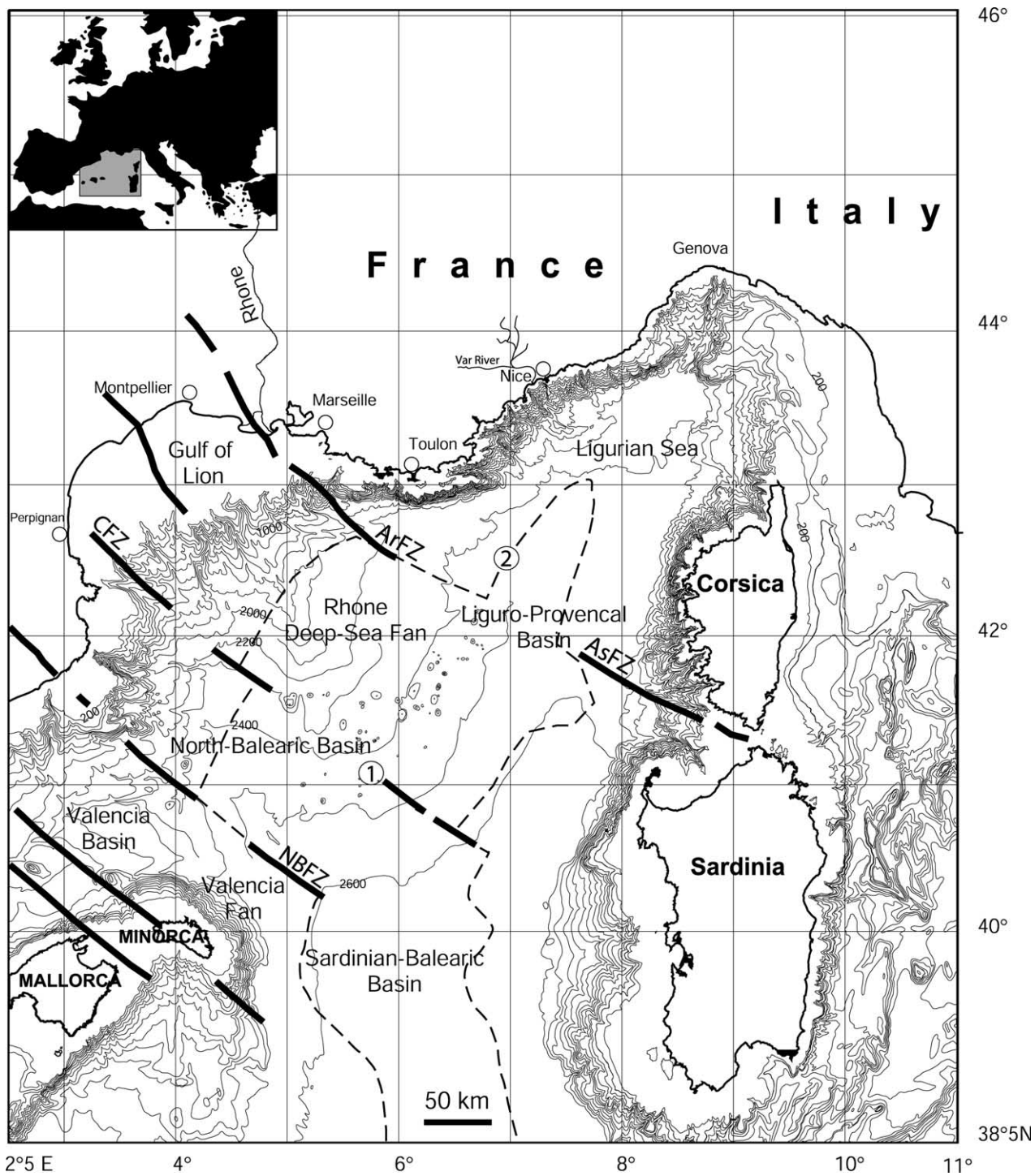


Fig. 1. Location of the study area and bathymetric map of the northwestern Mediterranean Basin. The abyssal plain is restricted to a northeast–southwest-trending depression that corresponds to the axial part of the Balearic-Provençal Basin. Numerous salt diapirs deform the middle and lower Rhône deep-sea fan. 1. Transfer zones; 2. Limit of the oceanic crust; ArFZ: Arlesian fracture zone; AsFZ: Asinara fracture zone; CFZ: Catalan fracture zone; NBFZ; North-Balearic fracture zone.

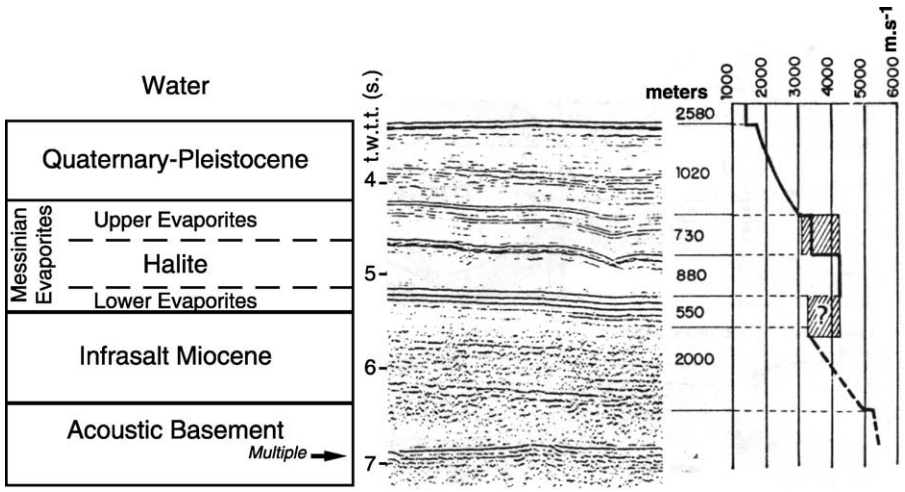


Fig. 2. Acoustic stratigraphy and seismic velocities of the sedimentary sequence in the northwestern Mediterranean Basin (modified from Réhault et al., 1984). The postrift sedimentary sequence in the basin includes the Messinian evaporites, which allowed for intense salt tectonics and diapirism.

comprises crustal-scale listric normal faults and half grabens in the continental crust underlying the upper shelf (Gorini, Mauffret, & Le Marrec, 1993). The shape of the margin was also influenced by recent deposition of thick clastic Plio-Pleistocene deposits of the Rhône deep-sea fan (Droz & Bellaiche, 1996). On the opposite side, the Corsica-Sardinia margin is a sediment-starved margin having a steeper continental slope (Bellaiche, 1993; Pautot, Bellaiche, Vanney, Rehault, & Coutelle, 1992; Rollet, 1999).

The sedimentary series in the Gulf of Lion can be subdivided into two main sequences (Fig. 2; Réhault et al., 1984), (1) an Oligocene-to-middle-Aquitanian synrift series present only between the tilted basement blocks and (2) a postrift sequence comprising upper-Aquitanian-to-Quaternary series. The postrift sequence deposited first the upper-Aquitanian to Tortonian series both on subsiding margins and in the deep part of the basin. Then the Messinian salinity crisis led to deposition of thick evaporites (including layers of halite) in the deep parts of the basin and to formation of a huge erosional unconformity on the basin's margins. Both the evaporitic layer and the unconformity are overlain by a Plio-Pleistocene sequence deposited after open marine conditions were reestablished in the Mediterranean (Fig. 2).

## 3. Structural pattern

### *3.1. Transverse basement faults or fault zones*

Seismic-reflection and magnetic data have indicated that the Ligurian-Provençal Basin contains several northwest-southeast-trending basement features. Each of these features corresponds to basement steps controlling the progressive deepening of the basin toward the center of the Gulf of Lion (Fig. 3; Chamot-Rooke, Gaulier & Jestin, 1997; Mauffret et al., 1995).

To the southwest, the North-Balearic fracture zone (Fig. 1), separating the basin from the Valencia trough, is characterized by strong magnetic anomalies (Galdéano & Rossignol, 1977), faults (Mauffret, Fail, Montadert, Sancho, & Winnock, 1973), and magmatic bodies (Maillard, 1993; Mauffret, 1976). This zone separates the Valencia trough, where the top of the acoustic basement is 4000 m deep, from the area northeast of the zone, where the basement is 5000–6000 m deep (Maillard et al., 1992). The seismic-reflection profile in Fig. 4 illustrates the time offset of about 1 s (TWT) across a zone of seismic diffraction where volcanic intrusions have been identified (Maillard & Mauffret, 1993). In this zone, the diffracting seismic character of both volcanic rocks and halite makes it is impossible to image clearly the faults of the fracture zone. However, the area of volcanic vents coincides with a break in regional basement dip, suggesting that the zone is a basement step. Fig. 4b (right-hand side) clearly shows presalt, Miocene reflectors onlapping on dipping, magmatic reflectors that terminate within the synrift sediments, indicating that part of the magmatic episode was syntectonic (Marti, Mitjavila, Roca, & Aparicio, 1992). However, volcanic rocks are also present near the top of Miocene sequence (Fig. 4a and other volcanoes in the Valencia trough).

Northward, the Catalan transverse fracture zone separates the Gulf of Lion from the Pyrenean belt (Gorini et al., 1993; Lefèvre, 1981; Mauffret, Durand, de Grossouvre, Gorini, & Nercessian, 2001). Interpretation of recent deep seismic data across this fault zone by Mauffret et al. (2001) and Nercessian et al. (2001) has evidenced crustal thinning accommodated by listric basement faults and an eastward deepening of the basement. This confirms the interpretation of the Catalan fracture zone as a basement step.

The northeast part of the Ligurian-Provençal Basin comprises two aligned fracture zones. The Arlesian fracture zone (Gorini et al., 1993; Mauffret & Gorini, 1996) bounds

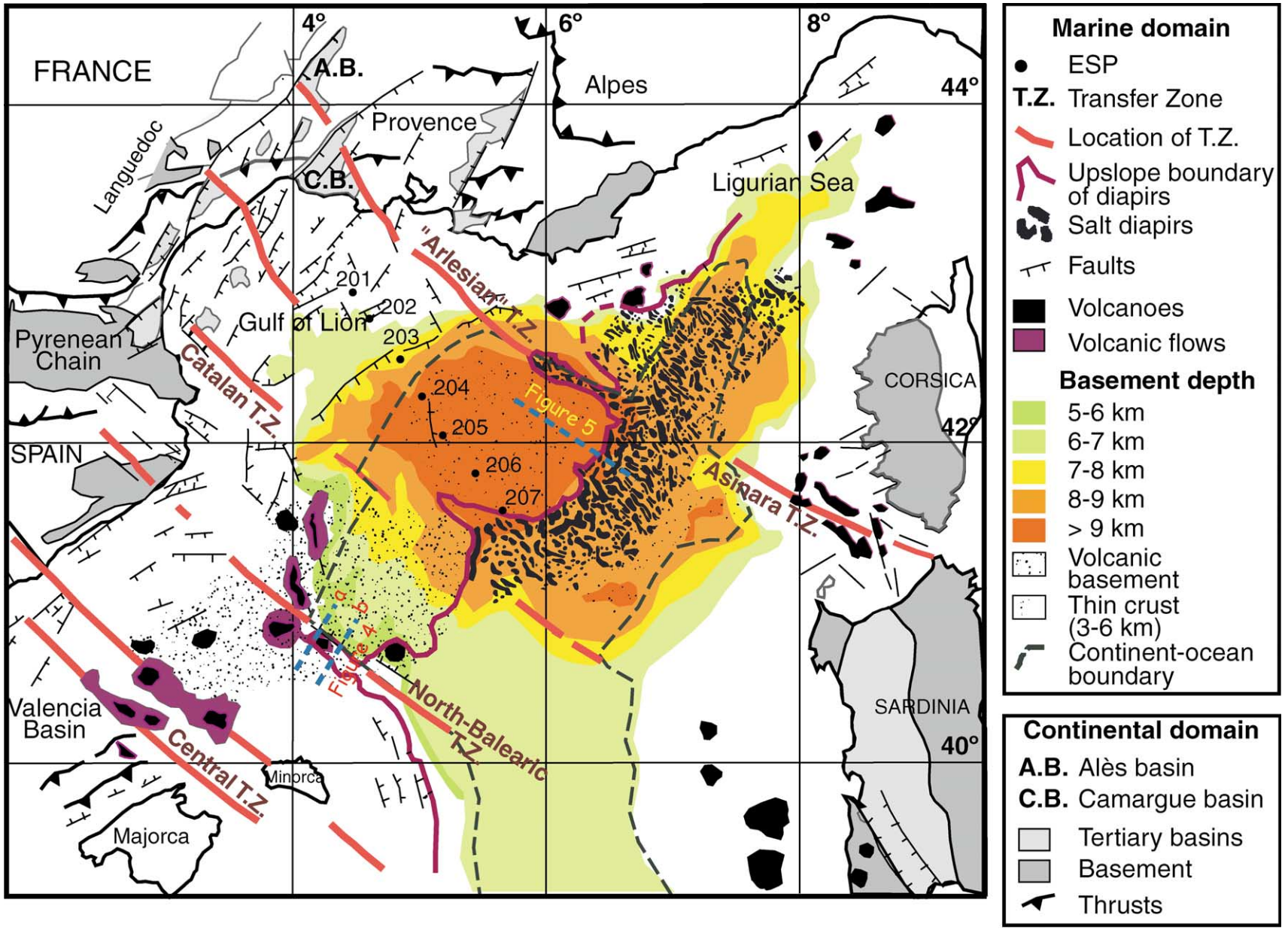


Fig. 3. Structural map of the northwestern Mediterranean Basin showing the upslope boundary of the area of Messinian salt diapirs and traces of the transfer zones overlain on the basement map. Detailed mapping reveals that although the upslope boundary of the diapir province trends northeast–southwest, perpendicular to the slope direction, the boundary also includes three northwest–southeast reentrants above the basement transfer zones. See text for explanations.

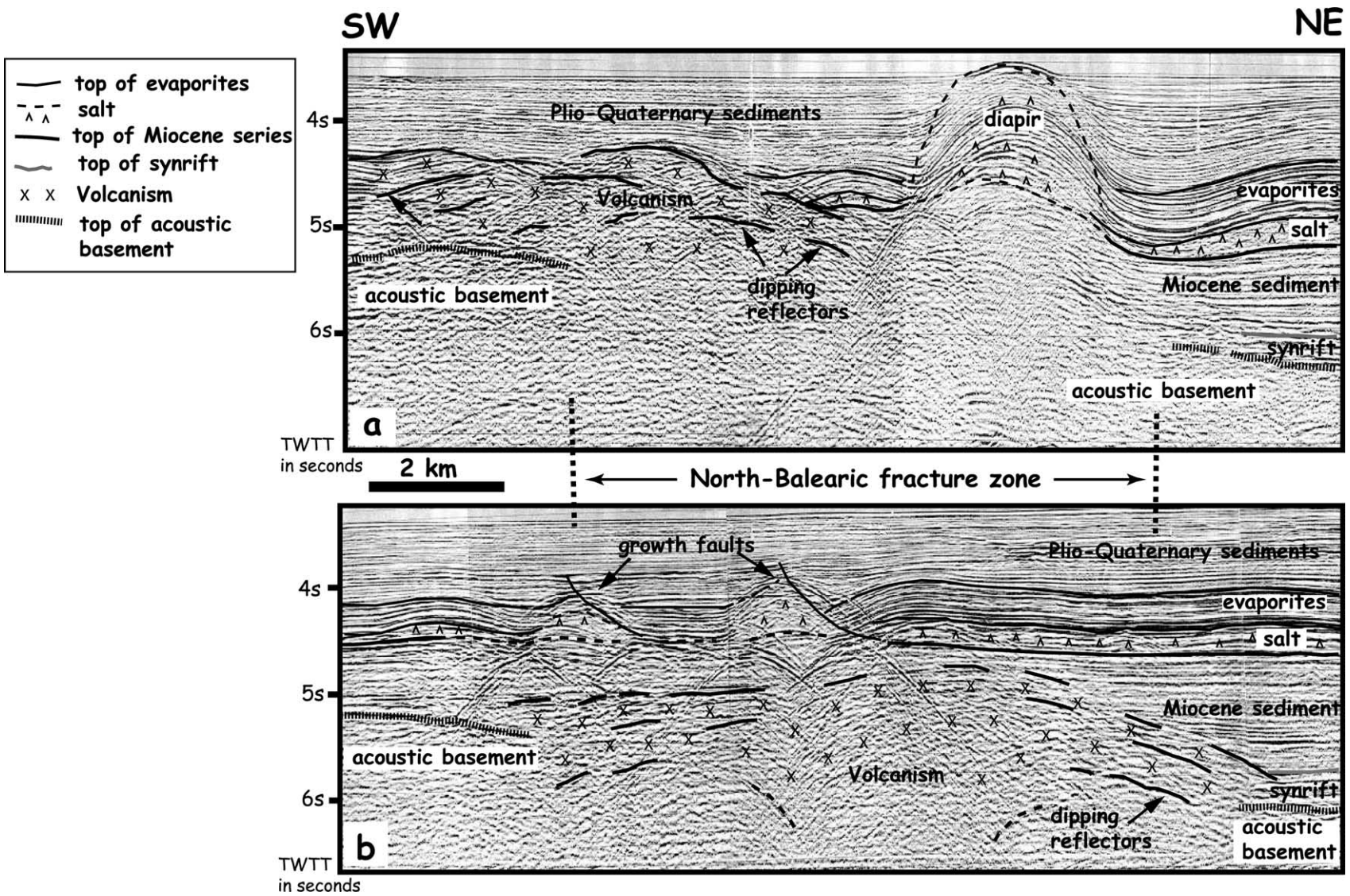


Fig. 4. Seismic-reflection profiles across the North-Balearic transfer zone (location on Fig. 3) showing that the northwest–southeast-trending fault zones are basement steps that control the basin's progressive deepening toward the center of the Gulf of Lion. The acoustic basement is offset on both sides of the transfer zone, where dipping reflectors are correlated with volcanic material (Maillard, 1993). The location of these basement transfer zones coincides with that of salt diapirs and growth faults.

the Gulf of Lion from the Ligurian Basin. The fracture zone forms a boundary between the thin, highly stretched continental crust of the Gulf of Lion (Pascal et al., 1993), where the top of the basement lies deeper than 5000 m beneath the continental shelf, and the thicker Provençal crust characterized by a narrow margin and a steep slope (Maillard & Mauffret, 1999; Mauffret et al., 1995). The Arlesian fracture zone continues toward the northwest (onshore) in the Camargue area (Seranne, Benedicto, Labaume, Truffert, & Pascal, 1995). Towards the southeast, it is located along the strike of the Asinara fracture zone (Auzende, Bonnin, & Olivet, 1973; Bayer, Le Mouël, & Le Pichon, 1973; Réhault et al., 1984). The latter is visible between Corsica and Sardinia by faults and magmatic lineations lying in the Bonifacio strait (Guennoc et al., 1998; Fig. 3).

Overall, the ocean–continent boundaries proposed by various authors (Bayer et al., 1973; Burrus, 1984; Mauffret et al., 1995; Réhault et al., 1984) are all offset by these northwest–southeast fracture zones, which therefore, can be interpreted as transfer zones that guided the opening of the basin and evolved into transform zones during seafloor spreading and are responsible for the complex structural and magnetic patterns in the oceanic crust (Gennesseaux, Réhault, & Thomas, 1989).

### 3.2. Distribution of salt structures

The Ligurian-Provençal Basin, especially in the Rhône deep-sea fan area, comprises numerous salt-related structures. Alinat and Cousteau (1962) were the first to suggest the presence of salt structures on the continental rise. Salt diapirs have circular or elongate (up to 15 km in length) planforms, and their crests can rise to 250 m above the seafloor (Pautot, Le Cann, Coutelle, & Mart, 1984). Formation of salt structures in the Ligurian-Provençal is attributed to combined gravity gliding and spreading of the Plio-Pleistocene overburden above the Messinian salt, which acted as a décollement (Gaullier, 1993; Gaullier & Bellaiche, 1996 and Dos Reis, 2001). Gravity gliding–spreading typically induces thin-skinned extension in the proximal (upslope) region, midslope translation, and distal (downslope) contraction (Fig. 5; Vendeville, in review). In the Ligurian-Provençal Basin, thin-skinned tectonics is characterized (1) by listric normal growth faults, salt rollers beneath fault footwalls, and rollover folds in the hanging walls in the proximal region, (2) by broad undulations in the midslope region, and (3) by salt-cored anticlines and diapirs in the downslope region (Gaullier & Bellaiche, 1996).

Mapping of the diapir distribution reveals that the updip boundary of the diapir region is generally perpendicular to the slope, hence trending northeast–southwest in the Ligurian-Provençal Basin (Gaullier, 1993) and north–south in the Balearic domain, except for three northwest–southeast-trending local reentrants. A first reentrant, located offshore of Toulon is aligned with the Arlesian basement fracture zone (Fig. 3; Gaullier, 1993). A second reentrant, mapped by Gaullier (1993) and Mauffret et al. (1995) using different seismic data sets, is located near the Catalan fracture zone. A third reentrant is aligned with the North-Balearic transfer zone. To the south, in the Valencia trough, diapirs are less developed because the evaporitic layer was initially thinner there.

### 3.3. Geographic correlation between subsalt and suprasalt structural features

Previous authors (Le Cann, 1987; Mauffret, 1976; Olivet, 1987; Pautot et al., 1984; Réhault et al., 1984) noticed the coincidence between the ocean–continent boundary and the edge of the diapir province in the Ligurian-Provençal Basin and have then used the latter as a marker for mapping crustal boundaries. Chamot-Rooke et al. (1997) reinterpreted results from seismic-refraction data and gravimetric modeling by Pascal, Mauffret, & Patriat (1993). Their results indicate that the limit of the diapir province in the central part of the basin coincides with the boundary between a very thin crust (thinner than 5 km), located between ESP 204 and ESP 207 (Fig. 3), whose oceanic affinity has not yet been demonstrated, from a thicker, typical oceanic crust south of ESP 207. The location of diapirs above the transverse basement structures was also noticed by Biju-Duval (1984), Mauffret (1976), and Sans and Sabat (1993). Fig. 3 clearly shows that the northwest–southeast reentrants of the diapir-province boundary are located near or immediately above the basement transfer zones, suggesting that there is a genetic relationship between the location of basement steps and the development of salt diapirs. Likewise, in the south part of the basin, the location of growth faults and diapirs appears to coincide with that of the underlying North-Balearic fracture zone. Faults and diapirs are usually located above the crest of magmatic bodies (Fig. 4). The base salt is offset by 0.2–0.3 s (TWT) across the North-Balearic fracture zone. The evaporitic layers are thicker in the northeast part of the fracture zone, owing to the deepening of the basement. The North-Balearic fracture zone, which marks the boundary between the aborted Valencia rift and the deep oceanic Provençal Basin, is also the limit of thick evaporitic deposits.

## 4. Possible mechanisms

Because of the geographic correlation between the location of basement transfer zones and that of the post-Messinian diapirs, Le Cann (1987) proposed that the basement structures were reactivated and therefore, influenced or controlled the formation of salt diapirs in the overlying cover. However, the timing of basement-fault reactivation does not match that of initiation and growth of salt diapirs in the area. Basement transfer zones were active during the Oligo–Miocene opening of

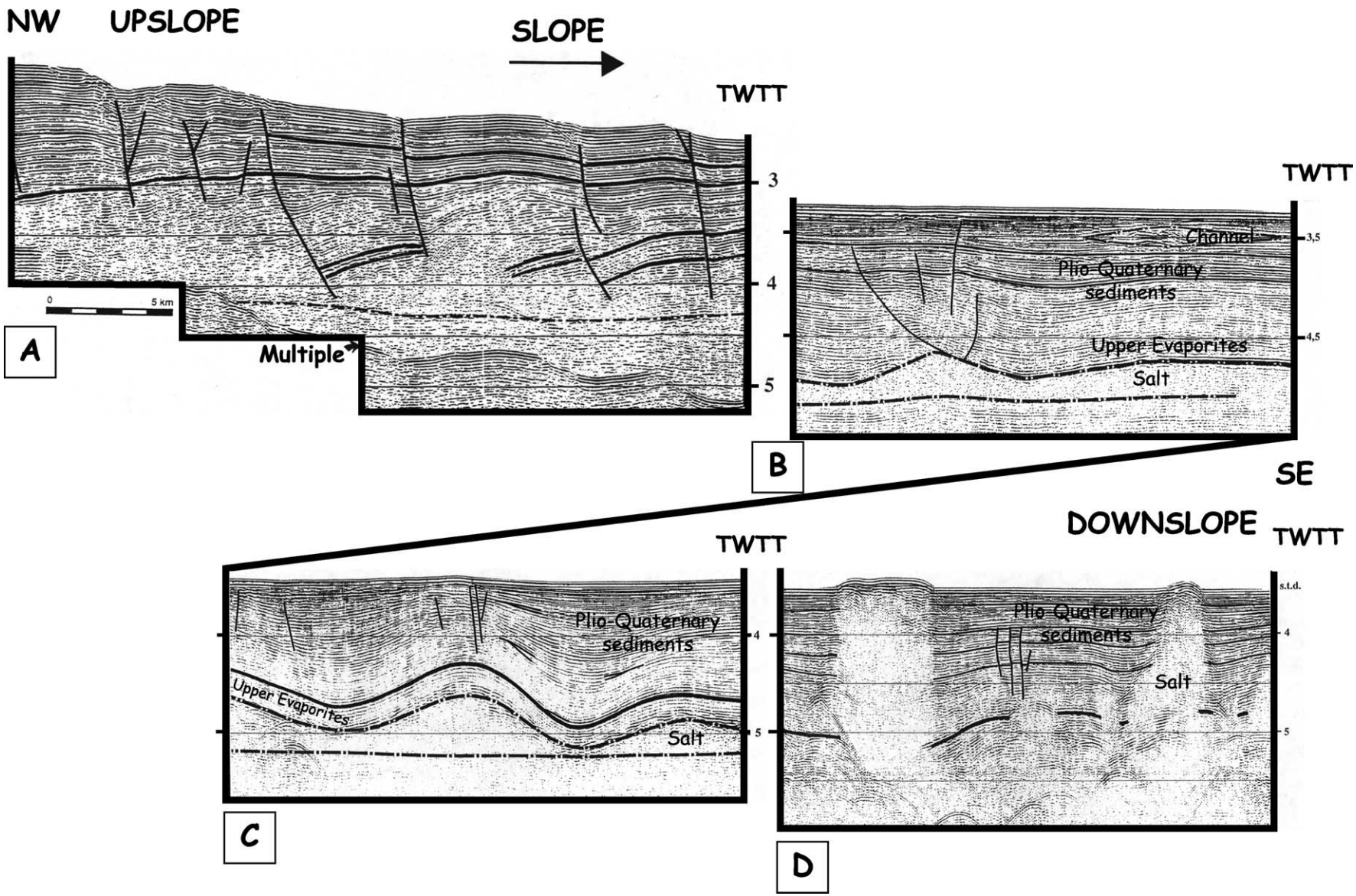


Fig. 5. Along-slope variations in structural styles of gravity-driven thin-skinned tectonics: A. Upslope extension: Listric normal growth faults associated with rollovers folds. B. Salt rollers and midslope translation. C. Salt anticlines. D. Downslope contraction and associated keystone grabens and diapirs. (Location on Fig. 3.)

the Ligurian-Provençal Basin (Bartrina, Cabrera, Jurado, Guimera, & Roca, 1992; Cravatte, Dufaure, Prim, & Rouaix, 1974), whereas diapir growth started, at the earliest, after deposition of the Messinian evaporites. In the northeast part of the region, there is no clear evidence of basement-fault reactivation coeval with growth of overlying salt structures. In the western part, Mauffret et al. (2001) have described that synrift faults on the western upper margin of the Gulf of Lion have been reactivated in extension during Late Miocene times. That fault reactivation is certainly related to the recent uplift onshore area. In the basin and in the Valencia Trough, however, crustal extension ceased after Langhian/Serravalian times, and this episode of fault reactivation is absent there.

These considerations suggest that the basement steps associated with the fault zones acted as dormant basement relief that affected the deformation pattern of the overlying Messinian evaporites and their Plio-Pleistocene sediment overburden. As pre-Messinian sediments filled the basement lows and reestablished a flat bathymetry, these sediments compacted under their own weight and the weight of the overlying Messinian and post-Messinian series. Because the pre-Messinian sediments compacted much more than basement rocks, the total amount of compaction varied laterally, from less above the basement highs to greater above the basement lows. After compaction, the geometry of the base-Messinian is expected to mimic partly the structural relief at the top of the basement.

Depending on the timing of differential compaction and rate of thin-skinned tectonics of the Plio-Pleistocene sediments, the structural relief at the base of the Messinian may have played either a passive or an active role. First, assuming that most of the compaction were to have occurred before significant thin-skinned extension began, the structural relief created by compaction played a passive role: gravity spreading–gliding of the evaporites and their overburden was affected by the base-salt relief, which partly controlled the location of faults and diapirs. Second, if most of the compaction had occurred during deposition and gliding–spreading of the Plio-Pleistocene sediments, the resulting flexure of the salt and overburden may have disturbed the stress field, hence the deformation pattern.

We used three physical experiments to test the influence of steps or flexure of the base salt, whether these form before or during deposition and gravity gliding–spreading of the overburden. First, we reviewed the results of an experiment by Gaullier, Brun, Guérin, & Lecanu (1993) modeling the passive influence of a dormant basement relief during gliding of the overlying salt-overburden system. Second, we used a compactable experimental material analogous to the pre-Messinian sediments in order to illustrate how basement relief is transmitted upward during differential compaction in the absence of salt tectonics. In the third experiment, we combined the effect of (1) compaction of pre-Messinian sediments and (2) gravity gliding of the Messinian and overburden series to illustrate the active influence of the base-salt relief created by compaction.

## 5. Experimental modeling

### *5.1. Experiment 1: Gravity gliding/spreading above a preexisting basement step (Figs. 6 and 7)*

In designing this experiment (Gaullier et al., 1993), we assumed that the base of the Messinian salt layer was initially offset by a dormant basement step inherited from the rifting stage (Fig. 6). The model was built in a box 80-cm long, 60-cm wide, and 12-cm high. The basement step trended 30° from the direction of the slope. After deposition of a viscous silicone layer (Silbione silicone, manufactured by Rhone-Poulenc, France), representing the Messinian evaporites, and a layer of dry sand, representing the brittle Plio-Pleistocene overburden, the entire model was tilted by 2.8°. Typically, tilting the model triggers downslope gliding (slope-parallel translation of the silicone and its overburden), characterized by proximal extension and, if the model is laterally confined, distal shortening. In addition, because the downslope part of the model comprised a free edge, no distal shortening took place. Instead, the model also deformed by spreading, a mechanism by which the lack of frontal buttress (i.e. low slope-parallel stress) triggers extension of the distal overburden.

Gravity spreading–gliding caused the formation of two families of faults (Fig. 6). The first family (90°; Fig. 6b and c) trended perpendicular to the slope, and faults were located in the upslope and downslope regions. These faults were associated with the updip and downdip edges of the models, both trending normal to the direction of the slope. Faults of the second family (Fig. 6b and c) trended parallel to the basement step (i.e. 30°) and were located above the basement step and in a triangular region on the downdip side of the basement step, where the viscous décollement layer was initially thicker. Faults formed preferentially on the downdip side of the basement step because gravity gliding–spreading was faster, hence the amount of extension greater, in areas where the viscous décollement was thicker. Fig. 7 shows how these oblique faults formed. During gliding, flow of the viscous source layer caused the overburden located above the step to flex, thus partly mimicking the topography of the underlying basement. A graben bounded by two normal faults formed in the upper hinge of the flexure, trending parallel to the basement step. A ridge of source layer rose reactively below the graben and eventually pierced the graben floor diapirically. Overall, the overburden flexure above the basement step localized the early formed faults and associated diapiric rise. Although no syntectonic sediments were added during this experiment, comparison with previously published modeling results (Guglielmo, Jackson, & Vendeville, 1997; Vendeville & Jackson, 1992)

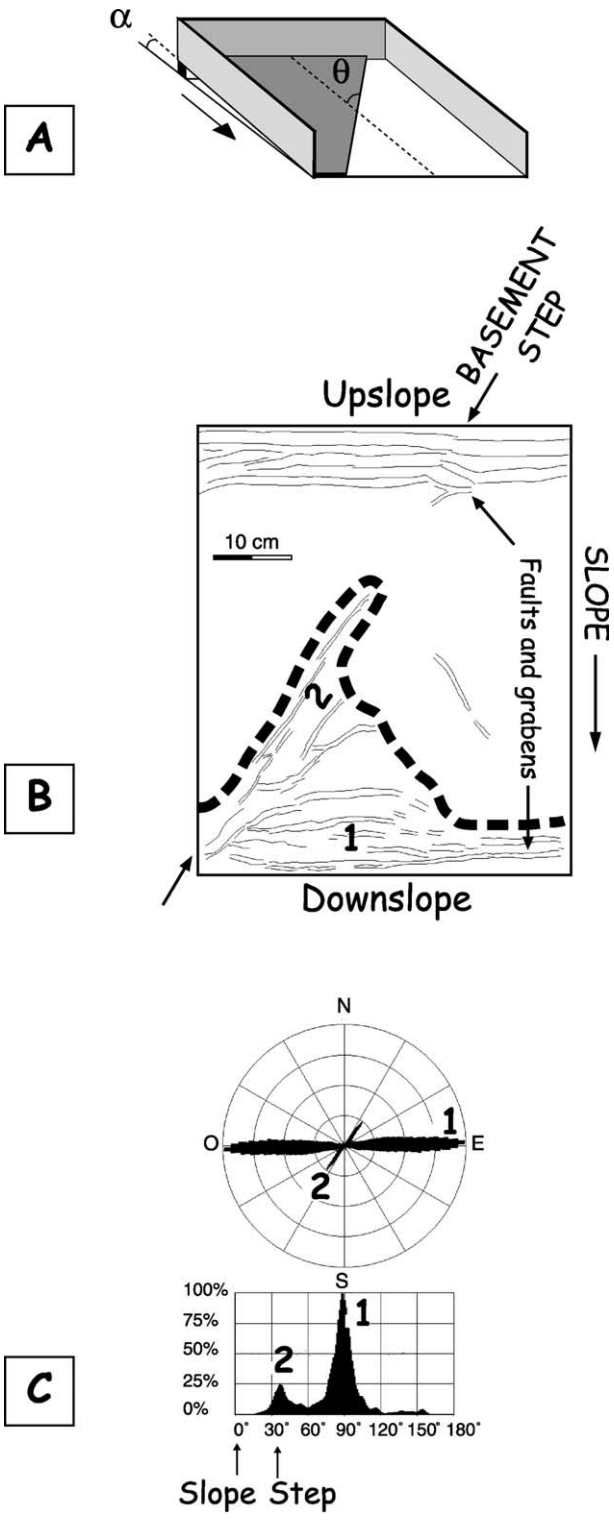


Fig. 6. Experiment 1: Results from a physical model of gravity-driven gliding–spreading by Gaullier et al. (1993). A: model set up. The regional slope, $\alpha$, was 2.8°; the angle between the slope and the basement step, $\theta$, was 30°. B: Line drawing of surface deformation showing that grabens and salt ridges are restricted to a triangular area bounded by the underlying basement step and encompassing the downdip part of the basement step. 1: 90° faults family; 2: 30° faults family. Black arrow indicates the trend of the step. C: Plot of fault orientations in the model illustrating the presence of two main fault families related to the upslope and downslope model's edges (1: 90° family) and to the basement step (2: 30° family).

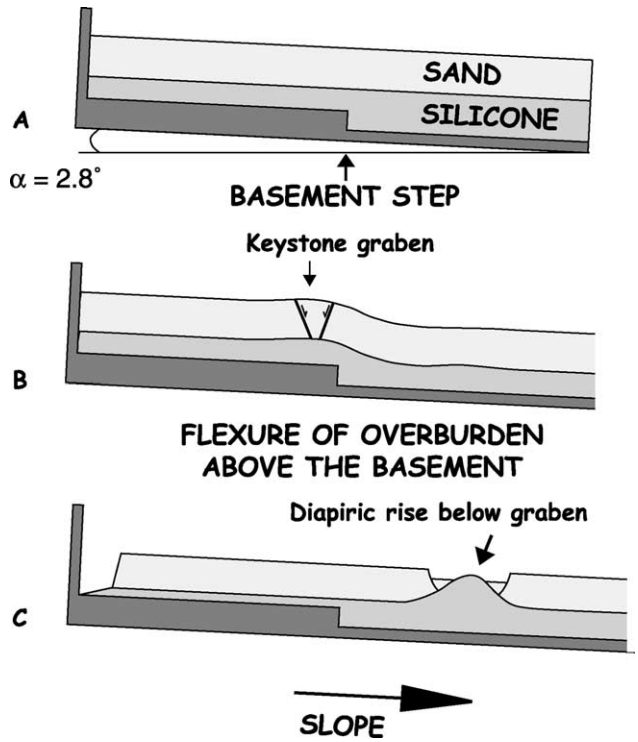


Fig. 7. Schematic cartoon showing the deformation pattern of the viscous décollement and brittle overburden during gliding above a basement step (from Gaullier et al., 1993).

suggests that such a set-up would have triggered the formation of diapiric stocks preferentially located in a reentrant aligned along the basement step, as observed in the Gulf of Lion.

### *5.2. Experiment 2: Upward propagation of dormant basement relief by differential compaction (Fig. 8)*

This experiment illustrates how differential compaction of pre-Messinian sediments can transmit a dormant, fault-controlled basement step into the Messinian and post-Messinian series. In this model, compaction started after deposition of the viscous décollement and its brittle overburden. The model was constructed in a $60 \times 42$ cm$^2$ box including a 6-cm-high basement step and overlain by a 7.4-cm layer of finely ground, compactable sand powder (representing pre-Messinian sediments). A 1.2-cm-thick layer of viscous silicone polymer (PDMS, a transparent Polydimethylsiloxane gum), representing the Messinian evaporites, and a 2.5-cm-thick dry quartz sand layer, representing the Plio-Pleistocene brittle cover, were deposited above the basement and the compactable layer before compaction began (Fig. 8a).

Compaction of the subsalt layer was achieved by removing the air within the fine-grained sand powder using a vacuum pump connected to the deformation box (Odonne, Ménard, Massonnat, & Rolando, 1999). The process lasted for about 3 h, beyond which insignificant additional compaction occurred.

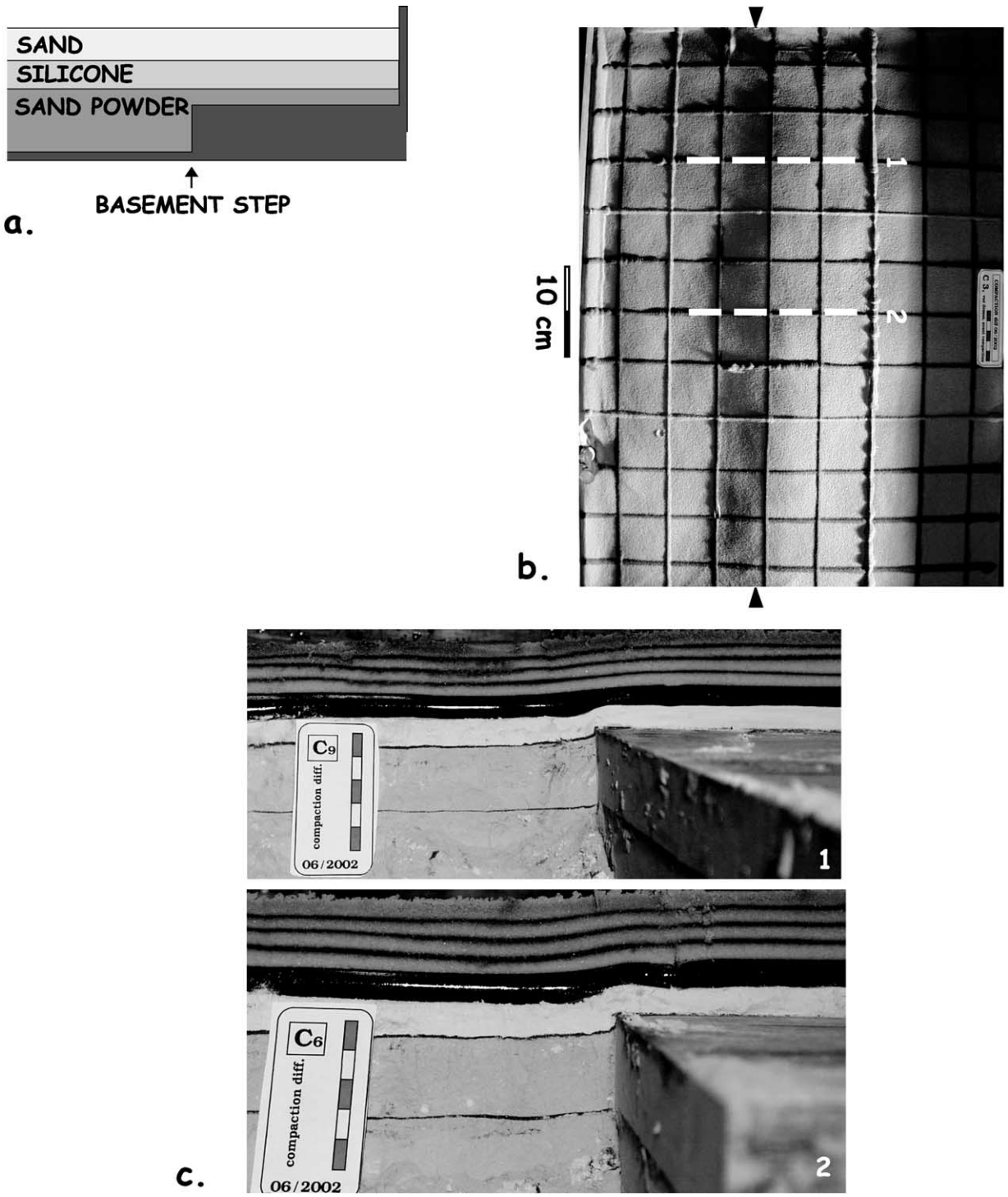


Fig. 8. Experiment 2: differential compaction above a basement step. The base of the viscous décollement was initially flat. (a) Experimental set up. (b) Overhead photograph of the model after deformation. The basement step trend is indicated by the solid black triangles, and the following cross sections by dashed white lines referenced 1 and 2. (c) Cross sections (located on Fig. 8b) showing the effects of a differential compaction above the basement step, including the offset of the silicone basement and the monoclinal flexure above the step. Scale bar = 5 cm.

Compaction caused the top of the fine-grained sand powder to subside more above the down side of basement step (where the layer was thickest) than on the up side of the step (Fig. 8b). This differential subsidence, in turn, partly transmitted the basement relief upward, forcing the overlying viscous layer and brittle overburden to bend and form a monoclinal flexure above the step (Fig. 8c). The resulting differential relief at the surface of the model (sand surface) comprised between 0.5 and 1 cm. In this experiment, because no lateral expansion was allowed, no

extension occurred (except for minor crestal stretching on the upper hinge of the flexure); hence no normal faults formed.

### 5.3. Experiment 3: Compaction-driven upward propagation of dormant basement relief during gravity gliding–spreading (Fig. 9)

This experiment illustrates how differential compaction of pre-Messinian sediments can transmit a dormant, fault-controlled basement step into the Messinian and control the location of suprasalt structures forming during gravity spreading–gliding.

The model was built and deformed in a 60 × 50 $cm^2$ box and comprised a 3-cm-high basement step 30° oblique to the direction of the slope (as in Model 1). The basement step was buried under a 4-cm-thick layer of compactable, fine-grained sand powder, representing the pre-Messinian sedimentary series, overlain by a 1-cm-thick layer of viscous silicone (PDMS), representing the Messinian evaporites, and a 1.2-cm-thick layer of dry quartz sand, representing the Plio-Pleistocene overburden (Fig. 9a). These materials had mechanical properties similar to those

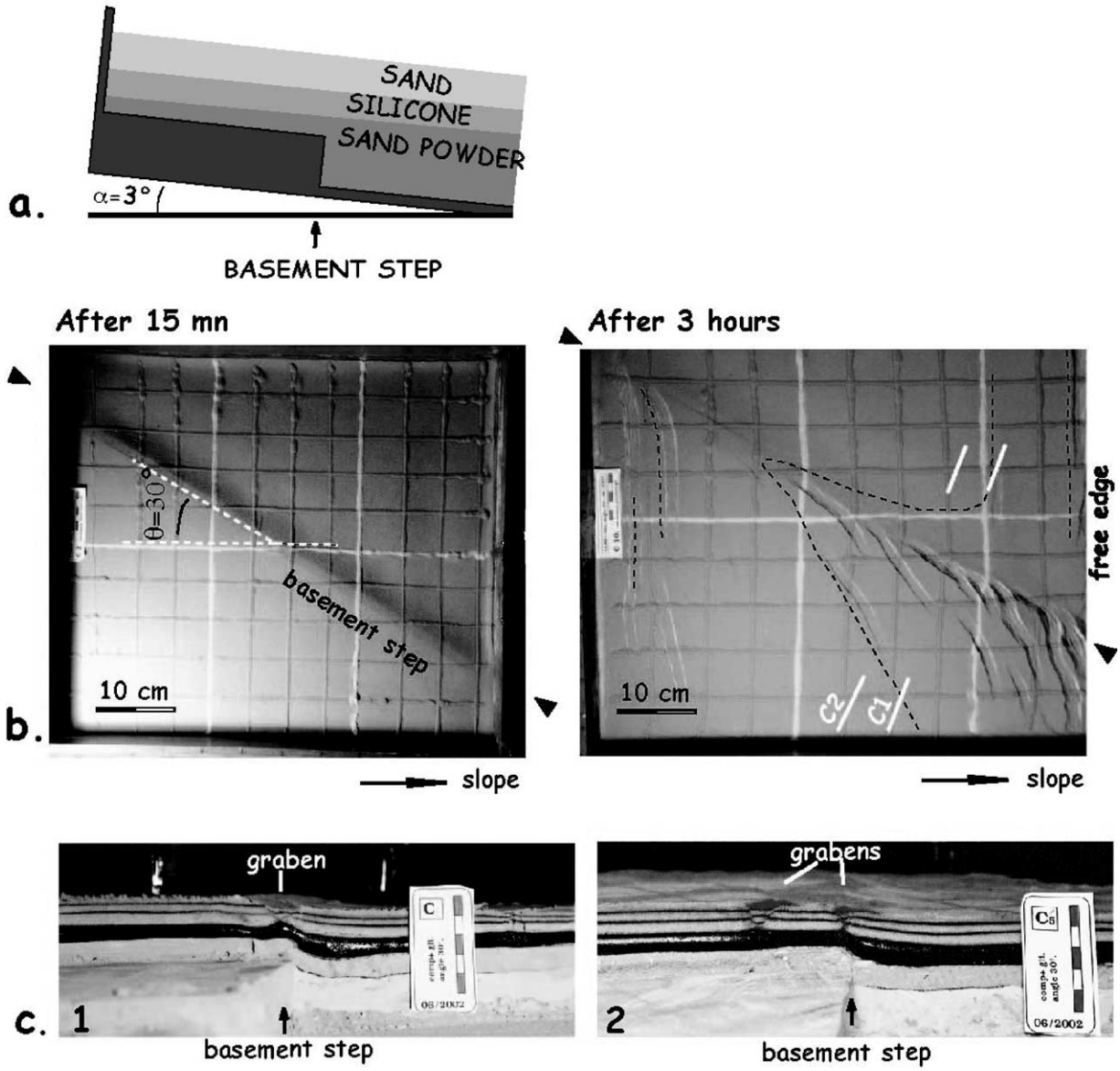


Fig. 9. Experiment 3: differential compaction above a basement step during gravitational gliding. The regional slope, $\alpha$, was 3°; the angle between the slope and the basement step, $\theta$, was 30°. (a) Experimental set-up. (b) Overhead photographs of the model after 15 min of deformation (compaction only) and after 3 h (compaction + gravity spreading–gliding). Black triangles indicate the location of the basement step (the structural high is located in the lower part of the photograph). White lines indicate the location of cross-sections shown on Fig. 9c. Dotted line: boundary of the graben province. Note that grabens and salt ridges are restricted to a triangular area bounded by the underlying basement step and encompassing the updip part of the basement step. (c) Cross-sections showing differential compaction above the basement step and detached grabens above the updip part of the basement step. Vertical bar = 5 cm.

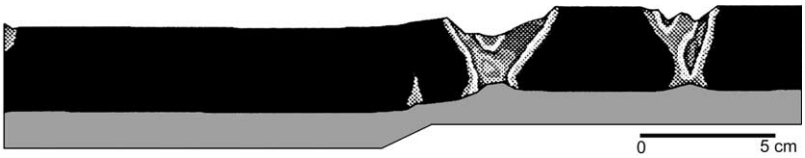


Fig. 10. Numerical model of deformation of viscous silicone (representing salt) and sand (representing a brittle overburden) above a basement normal fault for 1.63 cm of fault throw at 1.3 cm $h^{-1}$ (from Bobineau, 1992). The viscous silicone is gray. Overburden color varies with the amount of plastic deformation: darker areas are not deformed, lighter areas have deformed more. Fault zones appear white.

used in Experiment 2. The fine-grained sand powder was compacted by progressively vacuuming the air from the layer. Model deformation started with a 15-minute-long episode, during which only compaction occurred without tilting of the model. No extension took place. After 15 min, the deformation box was tilted and its down-slope endwall removed in order to trigger gravity gliding of the overburden while depletion and compaction of the fine-grained powder continued for an hour.

The overhead photograph shot after 15 min of compaction (Fig. 9b) shows a flexure located above the basement step. This observation indicates that differential compaction had already partly transmitted the basement offset upward, into the overlying viscous décollement and brittle overburden. Because no lateral movement was allowed during this episode, only minor extension occurred, being restricted to the formation of a small crestal graben above the basement step, near the updip edge of the model.

Tilting and removal of the downdip endwall of the box triggered downslope gliding of the brittle overburden. Gliding was mostly accommodated by downslope translation of the overburden and by formation of normal faults near the updip edge of the model. The overburden located on the down side of the basement step was translated downslope rigidly and was not faulted. As compaction and gliding progressed (Fig. 9b and c), a new generation of grabens formed in a triangular region located in the downdip part of the model, above the higher basement block. These grabens had arcuate traces. During the early stage of the experiment (first half-hour), the grabens formed parallel to and above the basement step. The grabens then propagated obliquely with a change in trend, their traces becoming subperpendicular to the regional direction of gliding–spreading. Overall, the area affected by graben faulting formed a reentrant whose apex followed the trend of the basement step.

In Model 1 (Fig. 7; Gaullier et al., 1993), grabens preferentially formed above the down side of the basement step. Grabens in Model 3 (Fig. 9), however, formed preferentially above the up side of the basement step (Fig. 9b and c). These differences can be explained as follows. In Model 1, which has a preexisting basement step, the viscous décollement layer had initially a flat top, and its thickness varied abruptly across the basement step. Consequently, faults formed above the down side of the basement step because there the décollement was thicker, gliding was faster, and the amount of extension greater. By contrast, the décollement layer in Model 3 was initially evenly thick, and its top and base were flat. During the first 15 min episode, when only compaction was applied and the overburden was not allowed to extend, compaction caused subsidence of the source layer and overburden above the down side of the basement step in a fashion similar to movement above a vertical basement fault. Because movements of the base of the décollement were only vertical and regional extension was absent, the overburden deformed mainly by monoclinal flexure. Analytical models by Couples (1977) have predicted that such a setting leads to principal stresses having curve trajectories. The stress field is extensional above the rising block and compressional above the subsiding block. During the following stage of deformation, however, the onset of gravity gliding changed the overall, regional stress field to extensional. This new, extensional regional stress field was superimposed onto the local extensional/compressional stress field associated with flexure of the base salt. Movement of the overburden became a combination of differential subsidence and lateral extension, a setting similar to that above a normal basement fault. Analytical, numerical, and physical models by Bobineau (1992), Koyi, Jenyon, and Petersen (1993), Koyi and Petersen (1993); Vendeville (1987, 1988), and Vendeville, Ge, and Jackson (1995) on salt tectonics above active basement faults have demonstrated that (1) subsidence of the down block (the basement hanging wall) triggers lateral salt flow from above the footwall toward the hanging wall and (2) grabens form preferentially above the footwall (Fig. 10) because this area is subjected to slightly greater extensional stresses.

Table 1
Summary of experimental conditions and parameters for each experiment

| Experiment No./Fig. | Basement step:height (cm) | Initial thickness of silicone (cm) | Sand thickness above silicone/ below silicone | Duration (h) |
|---|---|---|---|---|
| 1/Fig. 6 | 0.5 | 0.45–0.95 | 1 cm/None | 6 |
| 2/Fig. 8 | 6 | 1.2 | 2.4 cm/1.4 and 7.4 cm | 1 |
| 3/Fig. 9 | 3 | 1 | 1 cm/1 and 4 cm | 3 |

## 6. Conclusions

Our experimental results demonstrate that the presence of dormant steps in the subsalt basement can affect deformation of the overlying salt and sediment overburden. Where the base salt is initially offset by the step before deposition of the sediment overburden (Model 1), faults form above and downdip from the step, in a triangular area shaped like a reentrant. Where the base of an initially flat salt layer is progressively offset by subsalt compaction occurring after deposition of the salt and its overburden (Model 3), faults form above and updip of the step, in a triangular area shaped like a reentrant. These two situations correspond to two end members of the process by which a basement step can influence salt tectonics. It is likely that in natural examples, such as the Gulf of Lion, the influence of basement steps is a combination of both processes. Deposition of both Messinian and post-Messinian sediments, and the resulting increase in lithostatic stress, must have caused a progressive increase in compaction of the subsalt sediments. The first post-Messinian sediments, being deposited above a salt layer having a flat base must have deformed by spreading–gliding in a way similar to that of Model 3. The younger, post-Messinian sediments, being deposited when the base salt had a significant offset must have deformed in a way closer to that of Model 1. The combination between the two deformation styles (Models 1 and 3) would lead to the formation of grabens and associated diapiric ridges located in a reentrant centered on the basement step and covering both its updip and downdip regions.

All these models comprised a relatively thick layer of brittle overburden deposited before deformation began. No additional layers were added during deformation. The resulting deformation pattern included sublinear grabens underlain by rising diapiric ridges. Modeling results by Vendeville and Jackson (1992) and Guglielmo et al. (1997) illustrate how this pattern would change if (1) deformation started when the suprasalt sediments were thin and (2) continuous sediment aggradation progressively thickened the overburden. Their models show that through time, salt flow tends to be concentrated along shorter segments of the salt ridges. The final geometry consists of isolated circular diapirs (salt stocks). The diapirs, rooted at depth into the older salt ridges, grew by maintaining their crests at or near the seafloor while new sediments accumulated around them (passive diapir growth). Applying these observations to our modeling results suggests that the combination of the influence of subsalt basement steps and passive diapir growth would lead to formation of circular salt stocks restricted to a reentrant centered on the basement step, a geometry similar to that observed in the Gulf of Lion.

This study provides a genetic explanation for the geographic correlation between suprasalt and subsalt structures in the Gulf of Lion. The genetic link between the two is the influence of differential compaction of subsalt sediments that transmit upward the basement topography and thereby influence the development of salt structures and overburden faults. There are, however, other mechanisms that may also have contributed to this correlation. Thermal anomalies associated with basement transfer zones may have influenced the development of salt structures. Such anomalies and high heat flows could be linked to recent magmatic events, such as those observed along the transfer zones (Fig. 4a; Foucher et al., 1992; Maillard & Mauffret, 1993). Reactivation of volcanoes is probable, as indicated by recent alkaline intrusions sampled in the Valencia trough, and suggests that the history of magmatic events stretches from early Miocene to Plio-quaternary times (Marti et al., 1992). Recent magmatic activity above fracture zones could thus be linked to reactivation of the deep faults. Jackson and Talbot (1986) suggested that temperature gradients may influence halokinesis because salt viscosity varies with varying temperature. The influence of such temperature changes is, however, no longer thought to be significant when compared with the control exerted by the much stronger sediment overburden (Weijermars, Jackson, & Vendeville, 1993).

Another geological parameter that could interfere with the formation of salt structure is the pattern of loading by deposition of the Plio-Pleistocene overburden sediments. The continental slope and rise of the northwest Mediterranean are shaped by numerous channel-levee complexes having various planform shapes and sizes, from the large Rhône or Valence deep-sea fans to the smaller sedimentary bodies, such as the Fonera, Pyreneo-Languedocian (Berné, Loubrieu, & the Calmar team, 1999), Marseille, Grand-Rhone, and Cassidagne Ridges (Dos Reis, 2001). Recent experimental modeling (Gaullier & Vendeville, in review; Vendeville, in review) shows that initial planform geometry of the sediment load directly influences the pattern of salt deformation and the location and distribution of associated salt diapirs. The pattern of sediment loading in the northwestern Mediterranean may be regarded as a potential ‘external’ process that may have also contributed to the shape of the diapir regions in the area.

## Acknowledgements

We thank Lana Dieterich for editing this manuscript, and H. Koyi and A. Mauffret for helpful comments in their reviews.

## References

Alinat, J., & Cousteau, J. Y. (1962). *Accidents de terrain en Mer de Ligurie. Océanographie géologique et géophysique de la méditerranée occidentale*, Villefranche-Sur-Mer: Colloque CNRS, pp. 121–123.

Auzende, J. M., Bonnin, J., & Olivet, J. (1973). The origin of the western Mediterranean basin. *Journal of the Geological Society of London*, *129*, 607–620.

Bartrina, M. T., Cabrera, L. L., Jurado, M. J., Guimera, J., & Roca, E. (1992). Cenozoic evolution of the central Catalan margin (Valencia Trough, western Mediterranean). In E. Banda, & P. Santanach (Eds.), *Geology and geophysics of the Valencia Through, western Mediterranean* (*Vol. 203*) (pp. 219–248). *Tectonophysics*.

Bayer, R., Le Mouël, J. L., & Le Pichon, X. (1973). Magnetic anomaly pattern in the Western Mediterranean. *Earth and Planetary Sciences Letters*, *12*, 168–176.

Bellaiche, G. (1993). Sedimentary mechanisms and underlying tectonics structures on the northwestern Mediterranean margin, as revealed by comprehensive bathymetric and seismic surveys. *Marine Geology*, *112*, 89–108.

Berné, S., Loubrieu, B., & the Calmar team, (1999). Canyons et processus sédimentaires récents sur la marge occidentale du golfe du Lion. Premiers résultats de la campagne Calmar. *Comptes Rendus de l'Académie des Sciences de Paris, série IIa*, *328*, 471–477.

Biju-Duval, B. (1984). Les marges continentales françaises autour de la Méditerranée. In G. Boillot, M. Montadert, L. Lemoine, & B. Biju-Duval (Eds.), *Les marges continentales actuelles et fossiles autour de la France* (pp. 249–333). Paris: Editions Masson.

Bobineau, J. P (1992). *Simulations numériques de phénomènes tectoniques*. PhD Thesis. Ecole Centrale de Paris, 423 p

Burrus, J. (1984). Contribution to a geodynamic synthesis of the Provençal Basin (North-Western Mediterranean). *Marine Geology*, *55*, 247–270.

Chamot-Rooke, N., Gaulier, J. M., & Jestin, F. (1997). Constraints on Moho depth and crustal thickness in the Liguro-Provençal basin from a 3D gravity inversion: geodynamic implications. *Revue de l'Institut Français du Pétrole*, *52*, 557–583.

Couples, G. (1977). Stress and shear fracture (fault) patterns resulting from a suite of complicated boundary conditions with applications to the Wind River Mountains. *Pure and Applied Geophysics*, *115*(1/2), 113–133.

Cravatte, J., Dufaure, P., Prim, M., & Rouaix, S. (1974). Les sondages du Golfe du Lion: stratigraphie et sédimentologie. *Notes et Mémoires de la Compagnie Française des Pétroles*, *2*, 209–274.

Dewey, J. F., Helman, M. L., Turco, E., Hutton, D. W. H., & Knott, S. D. (1989). Kinematics of the western Mediterranean. In M. P. Coward, & D. Dietrich (Eds.), *Alpine tectonics* (*Vol. 45*) (pp. 265–283). *Geological Society of London Special Publication*.

Doglioni, C., Gueguen, E., Harabaglia, P., & Mongelli, F. (1999). On the origin of west-directed subduction zones and applications to the western Mediterranean. In B. Durand, L. Jolivet, F. Horvarth, & M. Seranne (Eds.), *The Mediterranean basins: Tertiary extension within the Alpine oragen* (*Vol. 156*) (pp. 541–561). *Geological Society of London Special Publication*.

Dos Reis, A. T (2001). *La tectonique salifère et son influence sur l'architecture sédimentaire quaternaire de la marge du Golfe du Lion en Méditerranée Occidentale*. Thèse de l'Université Paris VI, 373 p

Droz, L., & Bellaiche, G. (1996). Rhone deep sea fan: morphostructure and growth pattern. *American Association Petroleum Geologists Bulletin*, *69*, 460–479.

Foucher, J. P., Mauffret, A., Steckler, M., Brunet, M. F., Maillard, A., Réhault, J. P., Alonso, B., Desegaulx, P., Murillas, J., & Ouillon, G. (1992). Heat flow in the Valencia Trough: geodynamic implications. In E. Banda, & P. Santanach (Eds.), *Geology and geophysics of the Valencia through, western Mediterranean* (*Vol. 203*) (pp. 77–98). *Tectonophysics*.

Galdeano, A., & Rossignol, J. C. (1977). Assemblage à altitude constante de cartes d'anomalie magnétiques couvrant l'ensemble du bassin occidental de la Méditerranée. *Bulletin de la Société Géologique de France*, *7*(19), 461–468.

Gaullier, V (1993). *Diapirisme salifère et dynamique sédimentaire dans le bassin Liguro-Provençal: données sismiques et modèles analogiques*. Thèse de l'Université Paris VI, 327 p

Gaullier, V., & Bellaiche, G. (1996). Diapirisme liguro-provençal: les effets d'une topographie résiduelle sous le sel messinien. Apports de la modélisation analogique. *Comptes Rendus de l'Académie des Sciences de Paris, série IIa*, *322*, 213–220.

Gaullier, V., Brun, J. P., Guérin, G., & Lecanu, H. (1993). The effect of residual topography below a salt décollement. *Tectonophysics*, *228*(3/4), 363–381.

Gaullier, V., Vendeville, B. C (in review). Salt tectonics driven by sediment progradation. Part 2: radial spreading of circular lobes. *American Association Petroleum Geologists Bulletin*

Gennesseaux, M., Réhault, J. P., & Thomas, B. (1989). La marge continentale de la Corse. *Bulletin de la Société Géologique de France*, *5*, 339–351.

Gorini, C., Mauffret, A., & Le Marrec, A. (1993). Structural and sedimentary history of the Gulf of Lion (Western Mediterranean), finding of the ECORS profiles and well log data. *Bulletin de la Société Géologique de France*, *164*, 353–363.

Gueguen, E (1996). *La Méditerranée occidentale, un véritable océan*. Thèse de doctorat de l'Université de Bretagne occidentale, 311 pp

Gueguen, E., Doglioni, C., & Fernandez, M. (1997). Lithospheric boudinage in the western backarc Mediterranean basins. *Terra Nova*, *9*, 184–187.

Guennoc, P., Réhault, J. P., Gilg-Capar, L., Deverchère, J., Rollet, N., Le Suavé, R (1998). Les marges ouest et nord de la Corse: nouvelle cartographie au 1/250000. *17ème Réunion des Sciences de la Terre*, Brest (France), 31 mars–3 avril, Résumés, 124

Guglielmo, Giovanni, Jr., Jackson, M. P. A., & Vendeville, B. C. (1997). Three-dimensional visualization of salt walls and associated fault systems. *American Association of Petroleum Geologists Bulletin*, *81*, 46–61.

Jackson, M. P. A., & Talbot, C. J. (1986). External shapes, strain rates, and dynamics of salt structures. *Geological Society of American Bulletin*, *97*(3), 305–323.

Koyi, H., Jenyon, M. K., & Petersen, K. (1993). The effect of basement faulting on diapirism. *Journal of Petroleum Geology*, *16*(3), 285–311.

Koyi, H., & Petersen, K. (1993). Influence of basement faults on the development of salt structures in the Danish Basin. *Marine and Petroleum Geology*, *10*(2), 82–94.

Le Cann, C (1987). *Le diapirisme dans le bassin liguro-provençal*, Thèse Université de Bretagne occidentale, 296 pp

Le Douaran, S., Burrus, J., & Avedik, F. (1984). Deep structure of the north-western Mediterranean basin: results of a two-ship seismic survey. *Marine Geology*, *55*, 325–334.

Lefebvre, D (1981). *Evolution morphologique et structurale du Golfe du Lion. Essai de traitement statistique des données*. Thèse de troisième cycle l'Université Paris 6, 163 p

Maillard, A (1993). *Structure et riftogenèse du golfe de Valence (Méditerranée Nord-Occidentale).* Thèse de doctorat de l'Université Paris 6, 288 p

Maillard, A., & Mauffret, A. (1993). Structure et volcanisme dans la fosse de Valence (Méditerranée Nord-occidentale). *Bulletin de la Société Géologique de France*, *164*, 338–365.

Maillard, A., & Mauffret, A. (1999). Crustal structure and riftogenesis of the Valencia Trough (north-western Mediterranean Sea). *Basin Research*, *11*(4), 357–379.

Maillard, A., Mauffret, A., Watts, A. B., Torne, M., Pascal, G., Buhl, P., & Pinet, B. (1992). Tertiary sedimentary history and structure of the Valencia Trough (Western Mediterranean). In E. Banda, & P. Santanach (Eds.), *Geology and geophysics of the Valencia through, western Mediterranean* (*203*) (pp. 57–76). *Tectonophysics*.

Malinverno, A., & Ryan, W. B. F. (1986). Extension in the Tyrrhenian sea and shortening in the Apennines as a result of migration driven by sinking of the lithosphere. *Tectonics*, *5*, 225–245.

Marti, J., Mitjavila, J., Roca, E., & Aparicio, A. (1992). Cenozoic magmatism of the Valencia Trough (western Mediterranean): relation between structural evolution and petrogenesis. In E. Banda, & P. Santanach (Eds.), *Geology and geophysics of the Valencia through, western Mediterranean* (*203*) (pp. 145–166). *Tectonophysics*.

Mauffret, A (1976). *Etude géodynamique de la marge des Iles Baléares*. Thèse de troisième cycle de l'Université Paris 6, 137 p

Mauffret, A., Durand de Grossouvre, B., Gorini, C., & Nercessian, A. (2001). Structural geometry in the eastern Pyrenees ans western Gulf of Lion (Western Mediterranean). *Journal of Structural Geology*, *23*(11), 1701–1726.

Mauffret, A., Fail, J. P., Montadert, L., Sancho, J., & Winnock, E. (1973). Northwestern Mediterranean sedimentary basin from seismic reflection profile. *American Association Petroleum Geologists Bulletin*, *57*(11), 2245–2262.

Mauffret, A., & Gorini, C. (1996). Structural style of the Camargue area and western Provençal basin (southeastern France): geodynamic consequences. *Tectonics*, *15*, 356–375.

Mauffret, A., Pascal, G., Maillard, A., & Gorini, C. (1995). Tectonics and deep structure of the north-western Mediterranean Basin. *Marine and Petroleum Geology*, *12*(6), 645–646.

Montigny, R., Edel, J. M., & Thuizat, R. (1981). Oligo–Miocene rotation of Sardinia: K–Ar ages and paleomagnetism data of tertiary volcanics. *Earth and Planetary Sciences Letters*, *54*, 261–271.

Nercessian, A., Mauffret, A., Dos Reis, A. T., Vidal, R., Gallart, J., & Diaz, J. (2001). Deep reflection seismic images of the crustal thinning in the eastern Pyrenees and western Gulf of Lion. *Journal of Geodynamics*, *31*, 211–225.

Odonne, F., Ménard, I., Massonnat, G. J., & Rolando, J. P. (1999). Abnormal reverse faulting above a depleting reservoir. *Geology*, *27*(2), 111–114.

Olivet, J. L. (1987). L'origine du bassin nord-occidental de la Méditerranée du point de vue de la cinematique des plaques. In J. Burrus, & J. L. Olivet (Eds.), (*Vol. 35941-1*) (pp. 10–49). *Profils ECORS golfe du Lion: rapport d'implantation*, Paris: Institut Français du Pétrole.

Olivet, J. L. (1996). La cinématique de la plaque ibérique. *Bulletin du Centre de Recherche et d'Exploration Production Elf Aquitaine*, *20*, 131–195.

Pascal, G., Mauffret, A., & Patriat, P. (1993). The ocean–continent boundary in the Gulf of Lion from analysis of expanding spread profiles and gravity modelling. *Geophysical Journal*, *113*, 701–726.

Pautot, G., Bellaiche, G., Vanney, J. R., Rehault, J. P., & Coutelle, A. (1992). Morphobathymétrie des marges de la Corse établie à l'aide d'un nouveau sondeur multifaisceaux. *C.R. Acad. Sci. Paris*, *314*(Série II), 603–610.

Pautot, G., Le Cann, C., Coutelle, A., & Mart, Y. (1984). Morphology and extension of the evaporitic structures of the liguro-provençal basin: new Seabeam data. *Marine Geology*, *55*, 387–409.

Réhault, J. P., Boillot, G., & Mauffret, A. (1984). The western Mediterranean Basin, geological evolution. *Marine Geology*, *55*, 447–477.

Rollet, N (1999). *Structures profondes et dynamique du Bassin Ligure et de ses marges*. Thèse de l'Université Pierre et Marie Curie, 292 p

Ryan, W. B. F., & Hsu, K. I. (1973) (*Vol. 13*). *Inital Report of the Deep Sea Drilling Project*, Washington DC: US Government Printing Office, 1447 p.

Sans, M., & Sabat, F. (1993). Pliocene salt rollers and synkinematic sediments in the northeast sector of the Valencia trough (western Mediterranean). *Bulletin de la Société Géologique de France*, *164*(2), 189–198.

Seranne, M., Benedicto, A., Labaume, P., Truffert, K., & Pascal, G. (1995). Structural style and evolution of the Gulf of Lion Oligo–Miocene rifting: role of the Pyrenean orogeny. *Marine and Petroleum Geology*, *12*, 809–820.

Speranza, F., Villa, I. M., Sagnotti, L., Florindo, F., Cosentino, D., Cipollari, P., & Mattei, M. (2002). Age of the Corsica-Sardinia rotation and Liguro-Provençal Basin spreading: new paleomagnetic and Ar/Ar evidence. *Tectonophysics*, *347*, 231–251.

Vendeville, B. C. (1987). Champs de failles et tectonique en extension: modélisation expérimentale. *Rennes, France, Mémoires du Centre Armoricain d'Etudes Structurales des Socles*, *15*, 392.

Vendeville, B. C. (1988). Modèles expérimentaux de fracturation de la couverture contrôlée par des failles normales dans le socle (Scale-models of basement-induced extension). *Comptes Rendus de l'Académie des Sciences de Paris*, *307*(Série II), 1013–1019.

Vendeville, B.C (in review) Salt tectonics driven by sediment progradation, part 1: mechanics and kinematics. American Association Petroleum Geologists Bulletin

Vendeville, B. C., Ge, H., & Jackson, M. P. A. (1995). Models of salt tectonics during basement extension. *Petroleum Geoscience*, *1*, 179–183.

Vendeville, B. C., & Jackson, M. P. A. (1992). The rise of diapirs during thin-skinned extension. *Marine and Petroleum Geology*, *9*(4), 331–353.

Vigliotti, L., & Langenheim, V. E. (1995). When did Sardinia stop rotating? New paleomagnetic results. *Terra Nova*, *7*, 424–435.

Weijermars, R., Jackson, M. P. A., & Vendeville, B. C. (1993). Rheological and tectonic modelling of salt provinces. *Tectonophysics*, *217*, 143–174.